International Journal of aeroacoustics volume 11 · number 1 · 2012– pages 1 – 24

Broadband combustion noise simulation of open non-premixed turbulent jet flames

Bernd Mühlbauer[a,*], Roland Ewert[b], Oliver Kornow[b] and Berthold Noll[a]

[a]German Aerospace Center (DLR), Institute of Combustion Technology, Pfaffenwaldring 38-40, 70569 Stuttgart, Germany

[b]German Aerospace Center (DLR), Institute of Aerodynamics and Flow Technology, Technical Acoustics, Lilienthalplatz 7, 38108 Braunschweig, Germany

ABSTRACT

Numerical broadband combustion noise simulations of open non-premixed turbulent jet flames applying the Random Particle-Mesh for Combustion Noise (RPM-CN) approach are presented. The RPM-CN approach is a hybrid Computational Fluid Dynamics/Computational Aeroacoustics (CFD/CAA) method for the numerical simulation of turbulent combustion noise, based on a stochastic source reconstruction in the time domain. The combustion noise sources are modeled on the basis of statistical turbulence quantities, for example achieved by a Reynolds averaged Navier-Stokes (RANS) simulation, using the Random Particle-Mesh (RPM) method. RPM generates a statistically stationary fluctuating sound source that satisfies prescribed one- and two-point statistics which implicitly specify the acoustic spectrum. Subsequently, the propagation of the combustion noise is computed by the numerical solution of the Linearized Euler Equations (LEE). The numerical approach is applied to the DLR-A, the DLR-B and the H3 flames. The open non-premixed turbulent jet flames differ in the mean jet exit velocity, therefore in their respective Reynolds number, and in the fuel composition. Computed radial profiles of the reacting flow field are compared to experimental data and discussed. Computed sound pressure level spectra of the DLR-A and DLR-B flames and acoustic intensity level spectra of the H3 flame at different microphone locations are presented and compared to measurements.

Key words: combustion noise, stochastic source reconstruction, turbulence

NOMENCLATURE

Latin symbols

$\hat{A}$	Amplitude
c	Constant
D	Diameter

*Corresponding author. *Email address:* Bernd.Muehlbauer@DLR.de (Bernd Mühlbauer).

$\mathcal{G}$	Spacial filter kernel
k	Turbulence kinetic energy
l	Length scale
n	Dimension
p	Pressure
q	Source term
Q	Fluctuating sound source
r	Random value
$\boldsymbol{r}$	Separation space
$\hat{R}$	Variance of the correlated quantity
$\mathcal{R}$	Cross-correlation
s	Random value
t	Time
T	Temperature
u	Velocity
$\mathcal{U}$	Spatial white-noise field
V	Volume
x	Cartesian coordinate

Greek symbols

α	Constant
β	Constant
δ	Dirac δ-function
ϵ	Turbulence eddy dissipation
γ	Heat capacity ratio
μ	Viscosity
ρ	Density
τ	Separation time
τ	Time scale
ξ	Spatio-temporal white-noise

Dimensionless numbers

Pr	Prandtl number
Re	Reynolds number

Abbreviations

APE-RF	Acoustic Perturbation Equations for Reacting Flows
APU	Auxiliary Power Units
CAA	Computational Aeroacoustics
CFD	Computational Fluid Dynamics
DLR	German Aerospace Center
DNC	Direct Noise Computation
LEE	Linearized Euler Equations
LES	Large Eddy Simulation
lhs	Left-hand side

PIANO	Perturbation Investigation of Aerodynamic Noise
PPP	Points Per Period
PPW	Points Per Wavelength
RANS	Reynolds averaged Navier-Stokes
rhs	Right-hand side
RMS	Root Mean Square
RPM	Random Particle-Mesh
RPM-CN	Random Particle-Mesh for Combustion Noise

1. INTRODUCTION

Direct noise computation (DNC) methods for broadband combustion noise have to solve the complete, fully coupled, and compressible balance equations to simulate the reacting flow and the acoustics simultaneously. The vastly different scales of the dynamics of turbulence, chemical reactions, and acoustics as well as the need for low dissipation and low dispersion high order discretization schemes and acoustic boundary conditions triggered the development of hybrid Computational Fluid Dynamics/Computational Aeroacoustics (CFD/CAA) approaches in previous investigations, where the combustion noise problem was split into a reacting flow part to be treated with CFD and a subsequent aeroacoustic simulation by means of CAA methods.

Currently, hybrid approaches for the numerical simulation of broadband combustion noise are applied primarily based on acoustic sources computed by Large Eddy Simulations (LES). Subsequently, the acoustic propagation is predicted by solving the Acoustic Perturbation Equations for Reacting Flows (APE-RF) [1] or wave equations [2, 3]. For sound propagation over larger distances, however, CAA methods based on a discretization of the simulation domain with spatial meshes become increasingly expensive. In case of larger propagation distances it is necessary to sample the unsteady acoustic data on a surface that surrounds the flame and extrapolate it with, e.g., analytical methods such as Kirchhoff's surface integral [4, 5] or a porous Ffowcs Williams and Hawkings methods into the far field [6]. Computationally more effcient methods of predicting combustion noise spectra arise from statistical noise theory [7]. These methods are based on a modeled source term to represent the fluctuating heat release [8, 9].

In a previous work [10] a novel, highly efficient, and accurate approach for the numerical simulation of broadband combustion noise was derived and evaluated. The so called Random Particle-Mesh for Combustion Noise (RPM-CN) approach is a hybrid CFD/CAA method, based on a stochastic source reconstruction in the time domain. The combustion noise sources are modeled based on statistical turbulence quantities, for example achieved by a Reynolds averaged Navier-Stokes (RANS) simulation, using the Random Particle-Mesh (RPM) method [11, 12, 13]. Subsequently, the propagation of the combustion noise is computed by the numerical solution of the Linearized Euler Equations (LEE). The validation of the RPM-CN approach was done using the DLR-A and DLR-B flames. The capability of the RPM method to reproduce the prescribed two-point correlations was demonstrated and a good realization of the target source variance by the RPM method was achieved. Additionally, the influence of the length and

time scaling parameters of the turbulence temperature fluctuations on the predicted sound pressure level spectra was demonstrated by sensitivity analyses. The finally computed sound pressure level spectra of the DLR-A and the DLR-B flames with calibrated model parameters were compared to measurements at one microphone position located next to the acoustic source region.

The objective of this work is the application of the RPM-CN approach [10] to three different open non-premixed turbulent jet flames. Here, the reacting flow, the generation, and the combustion noise propagation of the DLR-A, DLR-B, and H3 flames is computed. The jet flames differ in the mean jet exit velocity, therefore in their respective Reynolds number, and in the fuel composition. First, in addition to the previous work [10], where the axial profile of the axial velocity, mixture fraction, temperature, and temperature RMS on the center line was evaluated, the radial profiles at different axial positions of the reacting flow simulation are compared to measurements for all flames. Subsequently, computed and measured broadband combustion noise spectra at different microphone positions of the DLR-A, DLR-B, and H3 flames are compared and discussed.

In section 2 the acoustic model and the modeling of the combustion noise source term of the RPM-CN approach is summarized. The experimental test cases are described in section 3 and the numerical configurations of the CFD and the CAA simulations are presented in section 4. In section 5 the results of the reacting flow and acoustic simulations are compared to the experimental data and discussed.

2. RPM-CN APPROACH

The Random Particle Mesh for Combustion Noise (RPM-CN) approach, a hybrid Computational Fluid Dynamics/Computational Aeroacoustics (CFD/CAA) method for the numerical simulation of turbulent combustion noise, is based on a stochastic source reconstruction in the time domain. There, the combustion noise sources are modeled on the basis of statistical turbulence quantities, for example achieved by a Reynolds averaged Navier-Stokes (RANS) simulation, using the Random Particle-Mesh (RPM) method. RPM generates a statistically stationary fluctuating sound source that satisfies prescribed one- and two-point statistics which implicitly specify the acoustic spectrum. Subsequently, the propagation of the combustion noise is computed by the numerical solution of the Linearized Euler Equations (LEE). The detailed derivation of the RPM-CN approach can be found in Ref. [10].

2.1. System of equations

The derived left hand side (lhs) of the pressure equation for reacting flows with a combustion noise source term on the right hand side (rhs) is equal to the lhs of the linearized Euler pressure equation and considered in combination with the continuity and the momentum equation of the genuine LEE. Hence, the acoustic model applied in this work is given by

$$\frac{\partial \rho'}{\partial t} + \tilde{\boldsymbol{u}} \cdot \boldsymbol{\nabla} \rho' + \boldsymbol{u}' \cdot \boldsymbol{\nabla} \overline{\rho} + \overline{\rho} \boldsymbol{\nabla} \cdot \boldsymbol{u}' + \rho' \boldsymbol{\nabla} \cdot \tilde{\boldsymbol{u}} = 0 \tag{1}$$

$$\frac{\partial \boldsymbol{u}'}{\partial t} + (\tilde{\boldsymbol{u}} \cdot \boldsymbol{\nabla})\boldsymbol{u}' + (\boldsymbol{u}' \cdot \boldsymbol{\nabla})\tilde{\boldsymbol{u}} + \frac{\boldsymbol{\nabla} p'}{\overline{\rho}} - \frac{\boldsymbol{\nabla}\overline{p}\rho'}{\overline{\rho}^2} = \boldsymbol{0} \tag{2}$$

$$\frac{\partial p'}{\partial t} + \tilde{\boldsymbol{u}} \cdot \boldsymbol{\nabla} p' + \boldsymbol{u}' \cdot \boldsymbol{\nabla}\overline{p} + \gamma\overline{p}\boldsymbol{\nabla} \cdot \boldsymbol{u}' + \gamma p'\boldsymbol{\nabla} \cdot \tilde{\boldsymbol{u}} = q_p \tag{3}$$

with the combustion noise source term

$$q_p = \frac{\overline{\gamma}\overline{p}}{\tilde{T}} \frac{\tilde{D}T''}{Dt}. \tag{4}$$

Here $D/Dt = \partial/\partial t + \boldsymbol{u} \cdot \boldsymbol{\nabla}$ denotes a substantial time derivative.

2.2. RPM method

The Random Particle-Mesh (RPM) method was introduced by Ewert [11, 12, 13] as a stochastic method to generate unsteady turbulent fields with locally prescribed one- and two-point statistics. The RPM method is an Eulerian-Lagrangian stochastic method, which generates a statistically stationary fluctuating sound source $Q(\boldsymbol{x},\ t)$ in the Eulerian frame used in CAA methods. The cross-covariance $\mathcal{R}$ generated by the method as applied in this work is Gaussian in space and exponential in time, i.e.

$$\begin{aligned} \mathcal{R}(\boldsymbol{x}, \boldsymbol{r}, \tau) &= \langle Q(\boldsymbol{x}, t) Q(\boldsymbol{x} + \boldsymbol{r}, t + \tau) \rangle \\ &= \hat{R}\ \exp\left\{ -\frac{|\tau|}{\tau_s} - \frac{\pi(\boldsymbol{r} - \boldsymbol{u}_c\tau)^2}{4l_s^2} \right\}, \end{aligned} \tag{5}$$

where $\langle \ldots \rangle$ denotes the ensemble average. $\hat{R}$ defines the variance of the correlated quantity for vanishing separation space $\boldsymbol{r}$ and time τ. The parameters l_s and τ_s denote integral length- and time scales, respectively. Taylor's hypothesis is taken into account by the convection velocity $\boldsymbol{u}_c$. For inhomogeneous turbulence $\hat{R},\ l_s,\ \tau_s$, and $\boldsymbol{u}_c$ depend on the position $\boldsymbol{x}$.

The fluctuating quantity $Q(\boldsymbol{x},\ t)$ is obtained by spatially filtering a spatial white-noise field $\mathcal{U}$

$$Q(\boldsymbol{x}, t) = \int_{V_s^n} \hat{A}(\boldsymbol{x}) \mathcal{G}(|\boldsymbol{x} - \boldsymbol{x}'|, l_s(\boldsymbol{x})) \mathcal{U}(\boldsymbol{x}', t) \mathrm{d}^n \boldsymbol{x}'. \tag{6}$$

In this expression $\mathcal{G}$ is a Gaussian spatial filter kernel defined by

$$\mathcal{G}(\xi, l_s) = \exp\left(-\frac{\pi}{2} \frac{\xi^2}{l_s^2} \right) \tag{7}$$

which yields a Gaussian spatial correlation of $Q(\boldsymbol{x},\ t)$, with integral length scale l_s. The dimension of the problem is indicated by n and V_S^n the source region. The amplitude function $\hat{A}$ realizes a local target variance of the fluctuating quantity $Q(\boldsymbol{x},\ t)$. The spatial white noise field $\mathcal{U}$ is generated by a Langevin equation [14]

$$\frac{D_0}{Dt}\mathcal{U} = -\frac{1}{\tau_s}\mathcal{U} + \sqrt{\frac{2}{\rho_0^c \tau_s}}\xi(\boldsymbol{x},t), \tag{8}$$

formulated in a Lagrangian frame. The quantity $\xi(\boldsymbol{x},t)$ is Gaussian distributed spatiotemporal white-noise, i.e. it satisfies

$$\langle \xi(\boldsymbol{x},t)\rangle = 0, \tag{9}$$

$$\langle \xi(\boldsymbol{x},t)\xi(\boldsymbol{x}+\boldsymbol{r},t+\tau)\rangle = \delta(\tau)\delta(\boldsymbol{r}), \tag{10}$$

where δ denotes the Dirac δ-function.

The convecting white noise field is modeled by convecting particles to discretize the filtered stochastic partial differential equation. Random values are associated to the particles, which are Gaussian deviates with a variance proportional to the inverse of the particle density. A bundle of streamlines covers the source domain that has to be resolved. Random particles are seeded at a constant clock rate at the foremost upstream position on each streamline. The particles drift along the streamline until they are finally removed downstream. The spatial filtering is applied sequentially. In the first step the random values are filtered along the streamline. Next, the values are weighted and distributed in direction normal to the streamline onto the CAA mesh.

To discretize the Langevin equation (8) the random values carried by each particle are not kept constant but rather change over time according to the discrete equation [15]

$$r_i^{n+1} = \alpha r_i^n + \beta s_i^n. \tag{11}$$

In this case r_i^{n+1} and r_i^n denote the random value of a particle at time-level $n+1$ and n, respectively. The quantity s_i^n is a Gaussian deviate with same variance as r_i. This procedure results to an exponential decay [16]. The constant α follows by discretizing the Langevin equation (8). It is related to the time-scale τ_s via

$$\alpha = 1 - \frac{\Delta t}{\tau_s}, \tag{12}$$

where Δt denotes the time-increment between the levels $n+1$ and n. To preserve the variance of r_i over time, β must be chosen as

$$\beta = \sqrt{\frac{2\Delta t}{\tau_s}}. \tag{13}$$

2.3. Statistical combustion noise source term modeling

The combustion noise source term q_p, Eq. (4), is modeled in accordance to the jet noise model of Tam & Auriault [17] where the two-point cross correlation of the substantial time derivative $\bar{D}q_s/Dt$ is modeled by

$$\left\langle \frac{\bar{D}q_s}{Dt}(\boldsymbol{x},t)\frac{\bar{D}q_s}{Dt}(\boldsymbol{x}+\boldsymbol{\xi},t+\tau)\right\rangle = \frac{A}{\tau_s^2}\exp\left\{-\frac{|\xi|}{u_c\tau_s}-\frac{\ln(2)}{l_s^{*2}}((\xi-u_c\tau)^2+\eta^2+\zeta^2)\right\}. \tag{14}$$

Here, the two-point cross-correlations of the substantial time derivative of the temperature fluctuations $\tilde{D}T''/Dt$ in Eq. (4) are modeled using the RPM method. The fluctuating quantity $Q(\boldsymbol{x},\ t)$, Eq. (6), represents the Favre fluctuations of the substantial time derivative of the temperature fluctuations $\tilde{D}T''/Dt$ and realizes Eq. (5).

The turbulent temperature length l_T and time scales τ_T for the combustion noise source term modeling might differ from the length l_s and time scales τ_s used for the Tam & Auriault jet noise model [17] in Eq. (14). This means that different calibration constants have to be applied. To clearly distinguish the turbulent temperature scales, the related parameters are labeled l_T, τ_T, c_{Tl}, and $c_{T\tau}$, instead of l_s, τ_s, c_l, and c_τ, in the following.

Hence, as an ansatz for the variance of the substantial time derivative of the temperature fluctuations, a term proportional to the variance of the Favre averaged temperature fluctuations divided by a turbulent temperature time scale τ_T squared is used. Furthermore an additional calibration constant c_q is considered, i.e.

$$\hat{R} = \frac{\widetilde{T''^2}}{c_q^2\tau_T^2}. \tag{15}$$

The modeled correlation function has three characteristic quantities, which are the length scale l_T and time scale τ_T of the turbulent temperature fluctuations as well as the temperature variance $\widetilde{T''^2}$. The turbulent temperature length l_T and time scale τ_T are linked to the turbulence model scales as a function of the turbulence kinetic energy k and the turbulence eddy dissipation ϵ by

$$l_T = c_{Tl}\frac{k^{3/2}}{\epsilon}, \tag{16}$$

$$\tau_T = c_{T\tau}\frac{k}{\epsilon}, \tag{17}$$

whereas the calibration constants c_{Tl} and $c_{T\tau}$ are introduced. For the computation of the temperature variance $\widetilde{T''^2}$ a transport equation [18] is solved

$$\frac{\partial \overline{\rho}\widetilde{T''^2}}{\partial t} + \frac{\partial \overline{\rho}\tilde{u}_j\widetilde{T''^2}}{\partial x_j} = \frac{\partial}{\partial x_j}\left\{\left(\overline{\mu} + \frac{\mu_t}{Pr_t}\right)\frac{\partial \widetilde{T''^2}}{\partial x_j}\right\} + c_{\text{prod}}\frac{\mu_t}{Pr_t}\left(\frac{\partial \widetilde{\overline{T}}}{\partial x_j}\right)^2 - c_{\text{diss}}\overline{\rho}\frac{\overline{\epsilon}}{\tilde{k}}\widetilde{T''^2}, \tag{18}$$

with $c_{\text{prod}} = 2.0$ and $c_{\text{diss}} = 2.0$.

To finally obtain the source term q_p, Eq. (4), the RPM generated source has to be complemented with the pre-factor $\overline{\gamma}\,\overline{p}\,/\,\widetilde{T}$, which deduces from the reacting RANS simulation.

3. EXPERIMENTAL TEST CASES

The investigated benchmark flames of the "International workshop on measurement and computation of turbulent non-premixed flames" [19] are open, non-premixed, turbulent jet flames and have the identical geometrical setup. The DLR-A and DLR-B flames are defined by the same nitrogen-diluted methane-hydrogen fuel mixture but differ in the mean jet exit velocity and therefore in their respective Reynolds number. In contrast, the H3 configuration is a nitrogen-diluted hydrogen jet flame and differs additionally in the mean jet exit velocity and its respective Reynolds number compared to the DLR flames.

The fuel is in all cases injected through a 0.35 m long straight stainless steel tube of diameter $D = 0.008$ m. The tube was surrounded by a contoured nozzle supplying co-flowing dry air. The outer nozzle had a diameter of 0.14 m. The fuel volume fractions, the stoichiometric mixture fraction, the mean jet exit velocity, the Reynolds number, and the mean coflow velocity of the flame configurations are listed in Table 1. Here, the Reynolds number is computed with respect to D, the mean jet exit velocity, and the kinematic viscosity of the fuel mixture.

The DLR flames have been experimentally investigated by Bergmann et al. [20], Meier et al. [21] and Schneider et al. [22] using Laser Doppler Anemometry (LDA),

Table 1: Parameters of the DLR-A, DLR-B, and H3 flames

	DLR-A	DLR-B	H3
ϕ_{CH_4}	22.1 Vol.%	22.1 Vol.%	–
ϕ_{H_2}	33.2 Vol.%	33.2 Vol.%	50 Vol.%
ϕ_{N_2}	44.7 Vol.%	44.7 Vol.%	50 Vol.%
$f_{st.}$	0.167	0.167	0.31
u_{jet}	42.15 m/s	63.2 m/s	34.8 m/s
Re	15200	22800	10000
u_{coflow}	0.3 m/s	0.3 m/s	0.2 m/s

Raman, Rayleigh scattering and Laser-Induced Fluorescence (LIF). Sound pressure level spectra were measured by Singh et al. [23]. LDA, Raman, Rayleigh scattering, and LIF were applied to the H3 configuration by Pfuderer et al. [24] and Tacke [25]. In contrast to the DLR flames, no measured sound pressure level spectra are available for the H3 configuration. However, acoustic intensity spectra were experimentally determined by Piscoya et al. [26].

4. NUMERICAL SETUPS

4.1. CFD setup

The CFD simulations were performed applying the commercial software package ANSYS CFX 11. For all configurations, the fully three dimensional computational domain was discretized with a cylindrical unstructured hexahedron mesh consisting of 370 000 nodes. The grid had dimensions of 94 D in axial and 113 D in radial direction and was strongly refined in the zones where strong gradients were expected. Furthermore, the growth of the adjacent cells was limited to 10%.

The fuel supply was modeled by a velocity inlet boundary condition. In the case of the DLR flames the measured velocity profile and profiles of the turbulence kinetic energy and the turbulence dissipation rate were specified at a temperature of 295 K. For the simulation of the H3 configuration computed profiles of the velocity, the turbulence kinetic energy and the turbulence dissipation rate of a LES [27] were specified at a temperature of 295 K. The coflow was defined by a mass flow of 5.5 g/s at a temperature of 295 K in all cases. The walls of the fuel pipe and the coflow were modeled by a adiabatic no-slip wall boundary condition. The free stream boundaries of the computational domain were approximated by a opening boundary condition. The option static pressure for entrainment, a static pressure of 0 Pa, and the zero gradient option for turbulence were applied [28].

A fully three dimensional compressible steady-state RANS simulation was performed to calculate the reacting flow field. The turbulence was considered by the Baseline Reynolds Stress Model (BSL-RSM) [28]. Chemical reactions were simulated applying the laminar Flamelet model [29], whereas the laminar flame speed was pre-calculated [30]. Additionally, a transport equation for the temperature variance, Eq. (18), was solved.

The fully implicit solver of ANSYS CFX 11 is based on a finite volume formulation for unstructured grids. The linear set of coupled equations was solved by a multigrid strategy. For the spacial discretization a High Resolution Scheme [31] was used. In this case a upwind scheme is used which is essentially second order accurate. Only for discontinuities the scheme switches to first order. Furthermore, buoyancy was taken into account by a source in the momentum equation, whereas heat radiation was neglected.

4.2. CAA setup

The stochastic reconstruction of the broadband combustion noise sources and the acoustic propagation were simulated using the DLR-CAA code Perturbation Investigation of Aerodynamic Noise (PIANO) [32]. Currently, the implementation of

the stochastic combustion noise source term reconstruction applying the RPM method is restricted to two dimensional plane modeling. Therefore, the computational CAA domain was discretized by a two dimensional plane block structured grid. The mesh covered 90 D in axial and 110 D in radial direction in the case of the DLR flames. For the simulation of the H3 flame the computational domain was extended to 94 D in axial and 138 D in radial direction to include the microphone locations of the measurements [26]. The computational meshes exist of 97 000 (DLR-A and DLR-B) and respectively 110 000 (H3) nodes. The grids were refined in the acoustic source zone and the growth of the adjacent cells was limited to 10%. All computational grids were appropriate to solve acoustic frequencies up to 11 000 Hz based on 7 Points Per Wavelength (PPW).

The acoustic propagation was computed by the numerical solution of the LEE. Acoustic non-reflective radiation boundary conditions by Tam & Webb [33] surrounded the computational domain. The PIANO code applies the fourth-order Dispersion-Relation-Preserving (DRP) scheme of Tam & Webb [33] in space and a fourth-order Low-Dissipation and Low-Dispersion Runge-Kutta (LDDRK) method [34] in time on block structured meshes. The time step size of $2 \cdot 10^{-6}$ s allowed a resolution of frequencies up to 71 000 Hz based on 7 Points Per Period (PPP). All simulations were conducted without filtering.

5. RESULTS

5.1. Reacting flow

In Fig. 1, 2, and 3 computed radial profiles of the axial velocity, the mixture fraction, the temperature, and the temperature Root Mean Square (RMS) of the DLR-A, DLR-B, and H3 flames are compared to the experimental data [20, 21, 22, 24, 25]. Measured axial velocity profiles of the DLR-B flame are not available. The reference diameter is the nozzle diameter $D = 0.008$ m and the mixture fraction was calculated using Bilgers definition [35]. Computed axial profiles at $r/D = 0$ of the DLR-A and the DLR-B flames have been already discussed in Ref. [10]. The agreement of the simulated radial profiles with the experimental data is similar for the DLR-A, DLR-B, and H3 flames. Therefore, in the following the computed radial profiles of the DLR-A flame are discussed exemplary.

Upstream, near the fuel exit $(x/D = 5)$ the computed axial velocity in Fig. 1a is in very good agreement with the measured profile. Further downstream $(x/D \geq 10)$ the computed jet is slightly more widened compared to measurements but the agreement of the simulated axial velocity profiles with the experimental data is still good. The computed radial profiles of the mixture fraction (Fig. 1b), temperature (Fig. 1c), and temperature RMS (Fig. 1d) show certain deviations to the measurements. The profiles at $x/D = 5$ indicate an over-prediction of mixing processes. The predicted shear layer seems so be wider in comparison with the experimental data. The simulated absolute temperature is in good agreement with measurements at all axial positions. Furthermore, the temperature RMS profiles computed by means of the temperature variance transport equation (18) do not reproduce the experimental profile exactly. But the predicted integral value of the temperature RMS is in good agreement with the measurements.

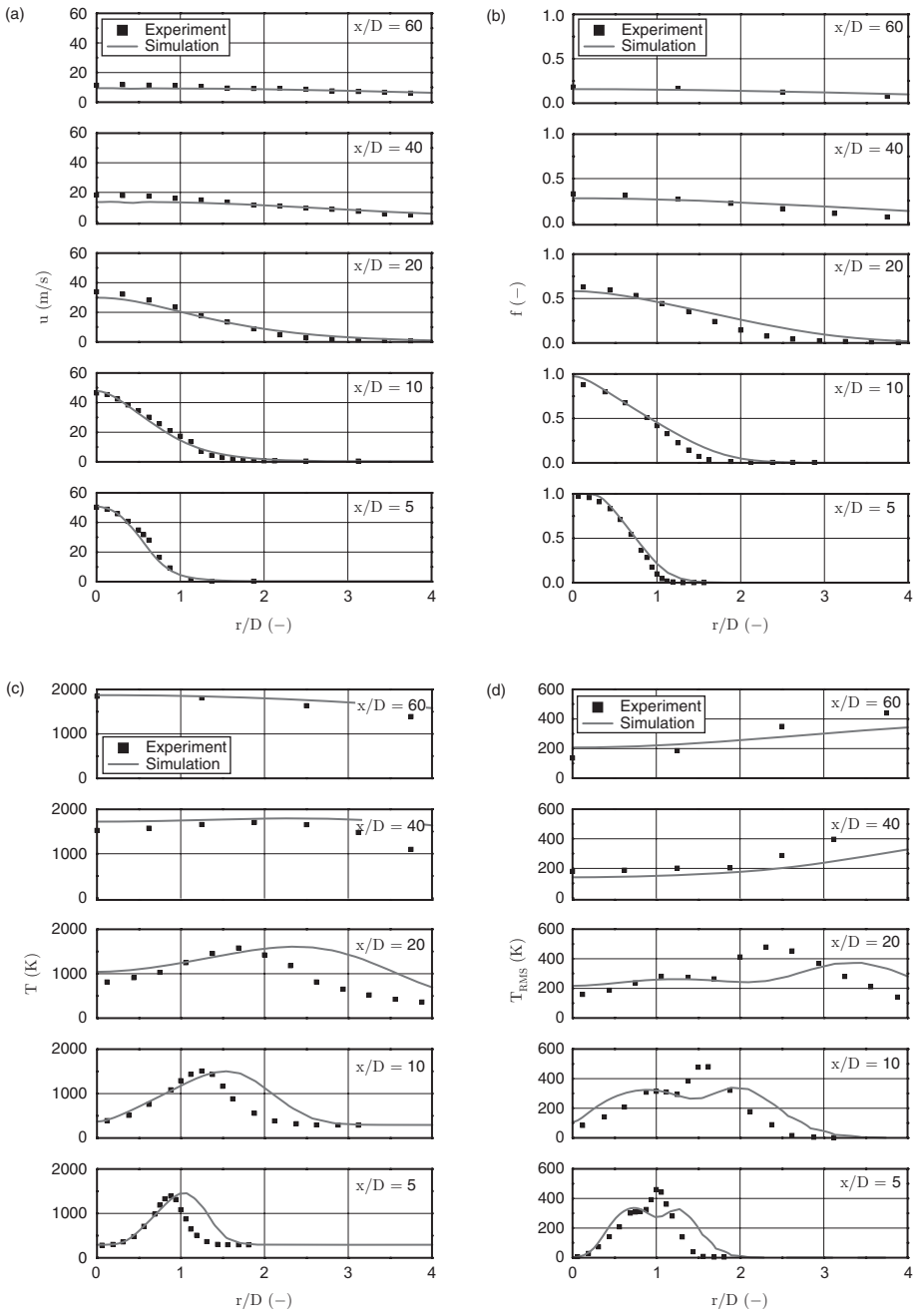

Figure 1: Measured and computed radial profiles of the DLR-A flame. (a) Axial velocity; (b) Mixture fraction; (c) Temperature; (d) Temperature RMS.

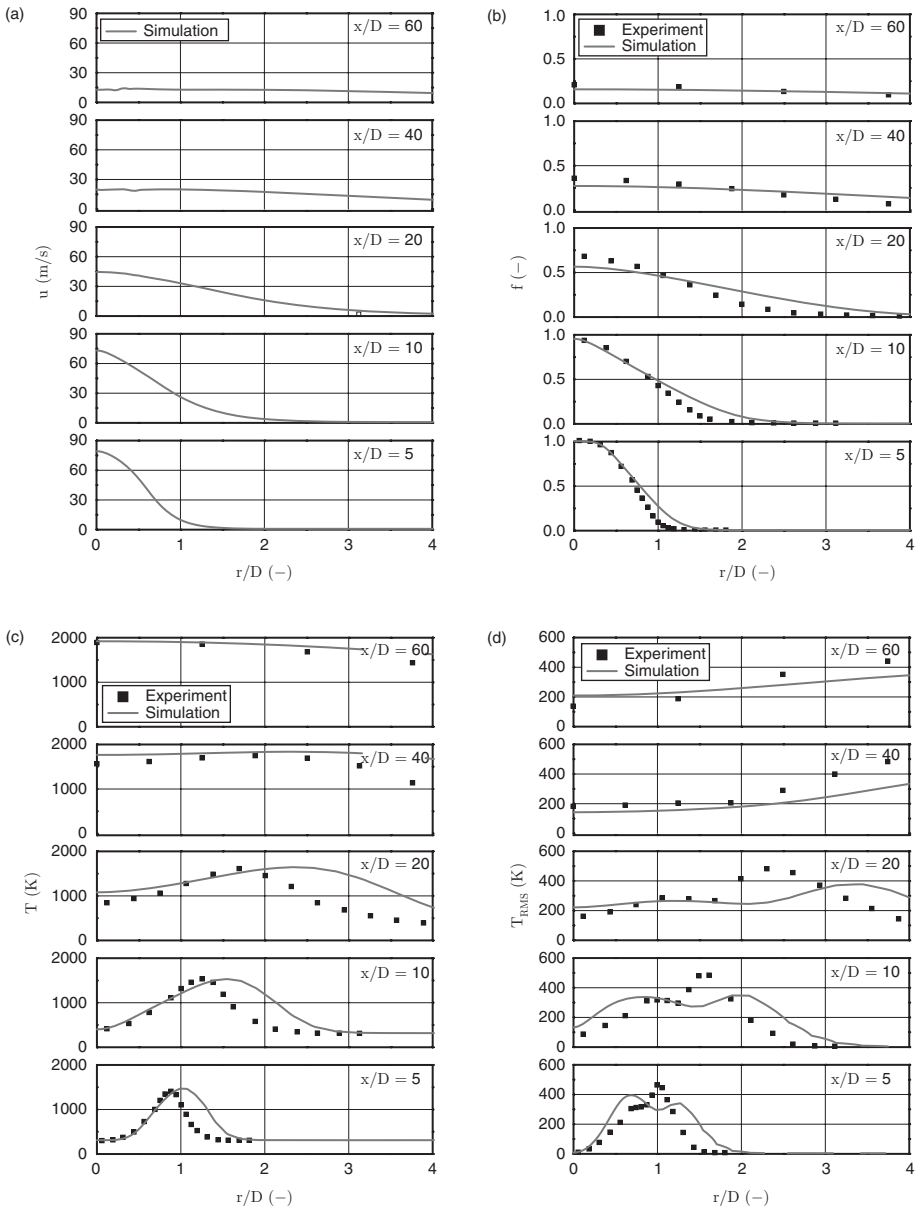

Figure 2: Measured and computed radial profiles of the DLR-B flame. (a) Axial velocity; (b) Mixture fraction; (c) Temperature; (d) Temperature RMS.

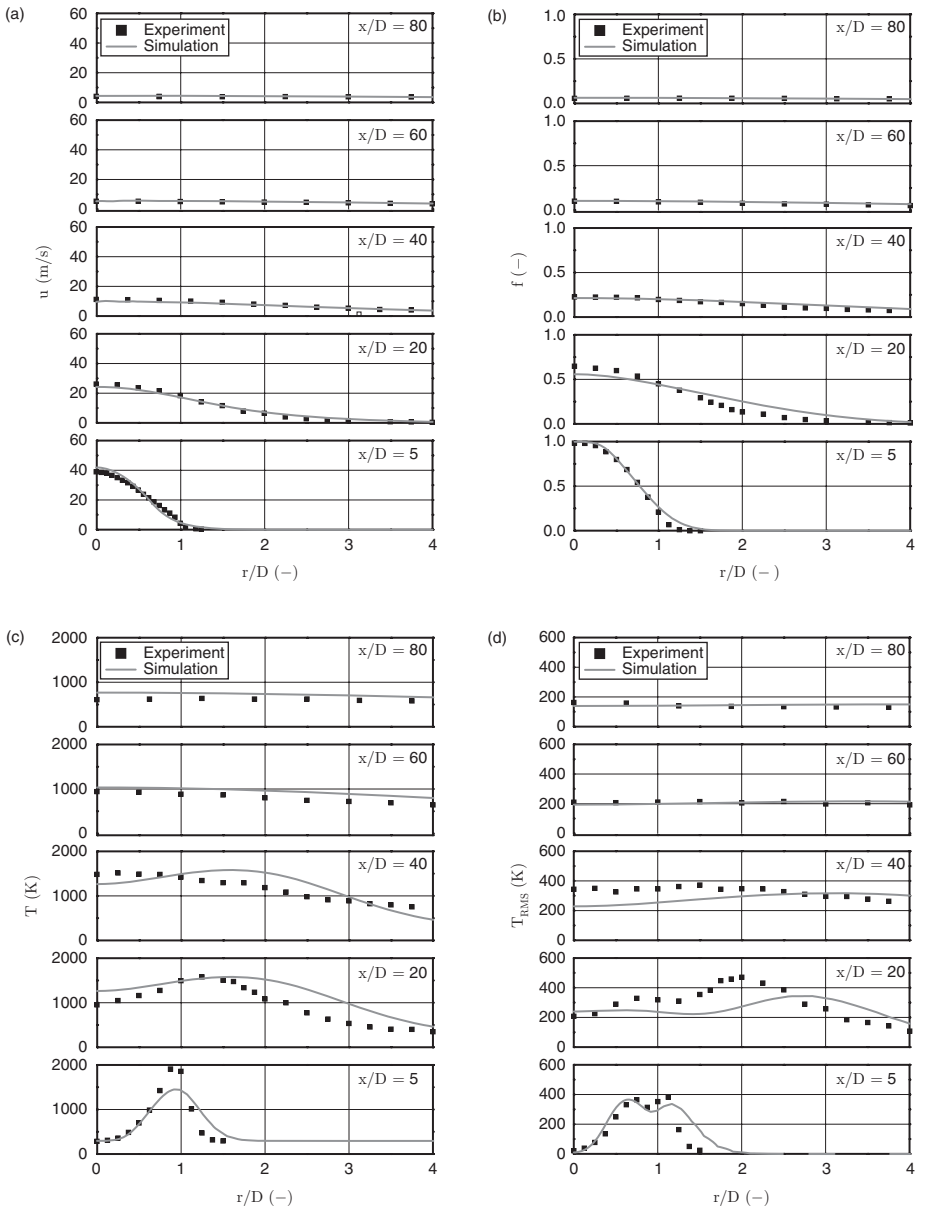

Figure 3: Measured and computed radial profiles of the H3 flame. (a) Axial velocity; (b) Mixture fraction; (c) Temperature; (d) Temperature RMS.

The results interpret a not exactly reproduction of the mixing processes due to the steady simulation and the simplified modeling of turbulent structures. Detailed investigations showed that the deviations of the simulated reacting flow field compared to the measurements are not dependent on the boundary conditions or on the quality of the combustion model. Simulations using a refined grid existing of 2 100 000 grid nodes did not show a relevant improvement concerning the agreement with measurements compared to the applied computational grid. Different further RANS turbulence models (k-ϵ, k-ω, and Shear Stress Transport) have been tested and it has been found that the applied BSL-RSM model provided the best results in these cases. The deviations of the temperature RMS profiles, compared to the experimental data can be attributed to the simplified turbulence and combustion modeling, since the temperature variance transport equation (18) is a function of the turbulence kinetic energy, the turbulence eddy dissipation, and the temperature. However, the applied RANS approach delivers acceptable results at low computational costs.

5.2. Acoustics

In a previous work [10] a parameter variation and calibration of the constants c_{Tl} and $c_{T\tau}$ which scale the length and time scale of the temperature fluctuations l_T and τ_T, Eq. (16) and (17), and the constant c_q which scales the amplitude $\hat{A}$, was done for two dimensional plane conditions using the DLR-A and DLR-B flames. Therefore, the combustion noise simulations presented in this work were performed using the parameters $c_{Tl} = 0.273$, $c_{T\tau} = 1.864$, and $c_q = 251.19$.

The computed sound pressure level spectra of the DLR-A and DLR-B flames which will be presented in the following were obtained by a Fast Fourier Transformation (FFT). The computed sound pressure fluctuations with a real time of 0.2 s were split into intervals and their spectral distribution was computed using an averaging procedure. According to the Nyquist-Shannon sampling theorem, the resolution of frequencies $f < 100$ Hz is excluded due to the length of the evaluated time signal. A narrow band spectrum of 25 Hz was chosen and the sound pressure level spectra are A-weighted decibel (dBA), both in accordance to the experimental data [23].

In Fig. 4, 5, 6, and 7 the computed sound pressure level spectra of the DLR-A and DLR-B flames are compared to the experimental data [23] at the microphone positions #1 to #9. The computed sound pressure level spectra at microphone position # 1 were already presented and discussed in Ref. [10]. The agreement of the computed sound pressure level spectra of the DLR-A and DLR-B flames with the experimental data is at all microphone locations comparable. The simulated sound pressure level spectra at the microphone position #1 are in very good agreement regarding the amplitude as well as the shape over the whole frequency range. At this point, a special emphasis has to be placed on the fact that the computed sound pressure level spectra are not shifted into each other. Since the simulations were done with the same parameter set, the very good agreement of the combustion noise simulation of the DLR-A as well as of the DLR-B flame with measurements demonstrates the independency of the numerical approach with respect to the Reynolds number.

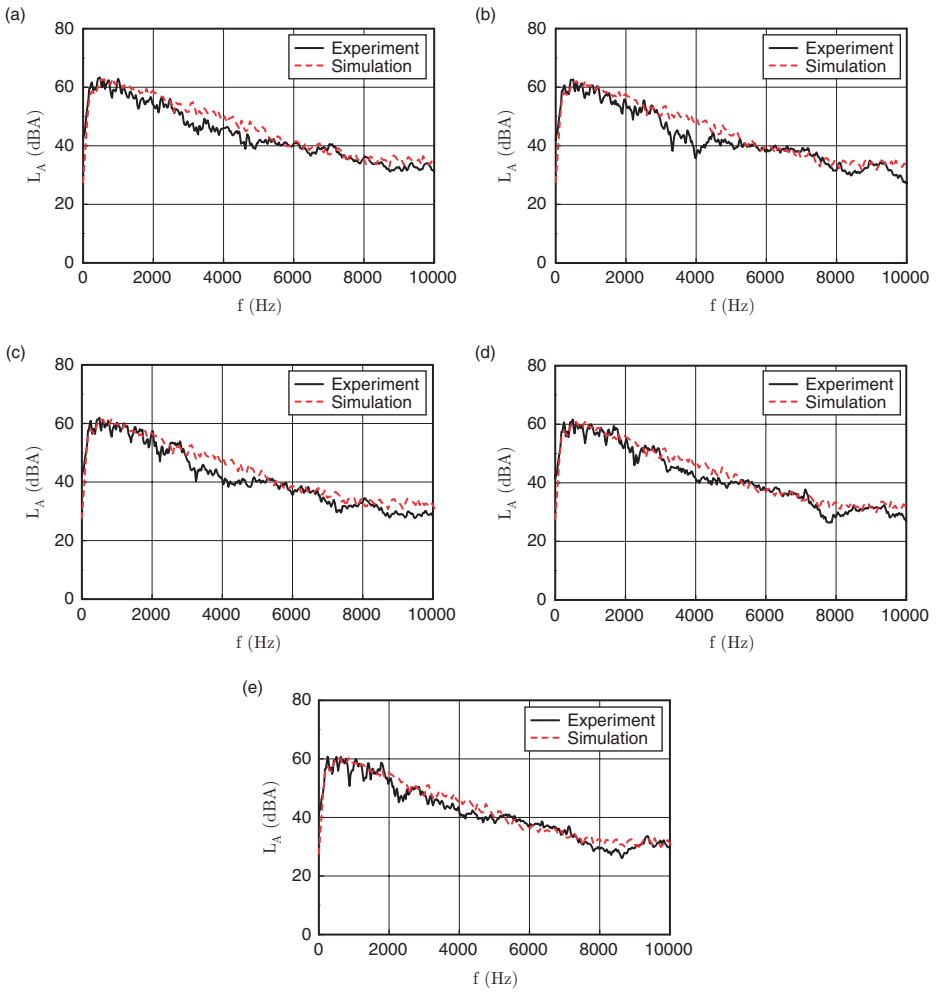

Figure 4: Measured and computed A-weighted sound pressure level spectra at the microphone positions #1 to #5 of the DLR-A flame. (a) #1 (25 D/0 D); (b) #2 (31 D/0 D); (c) #3 (37 D/0 D); (d) #4 (43 D/0 D); (e) #5 (50 D/0 D).

All computed sound pressure level spectra at the further microphones located in the fuel exit plane (#2 to #5) are in very good accordance with measurements as well, Fig. 4 and 6. The modeled radial decline of the acoustic pressure does not exactly correspond to the physics because of the two dimensional plane approximation. However, due to the short radial propagation distances this point shows no crucial impact on the simulated sound pressure level spectra.

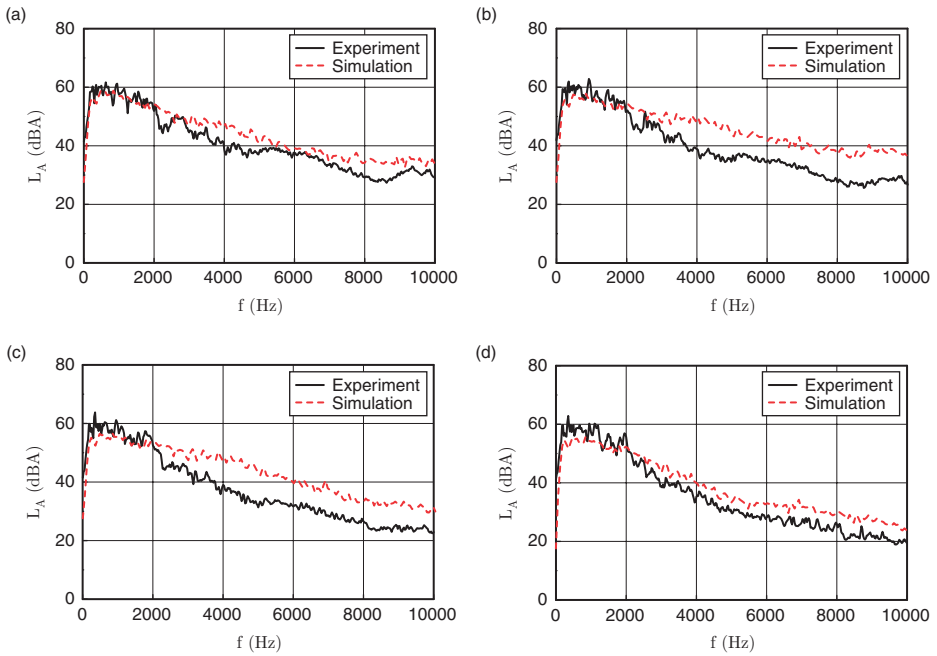

Figure 5: Measured and computed A-weighted sound pressure level spectra at the microphone positions #6 to #9 of the DLR-A flame. (a) #6 (50 D/12 D); (b) #7 (50 D/25 D); (c) #8 (50 D/37 D); (d) #9 (50 D/50 D).

The computed sound pressure level spectra at the microphone locations #6 to #9 which are distributed further downstream show certain deviations compared to the experimental data. In the low frequency range $f < 2000$ Hz the computed spectra are slightly under predicted and the spectra show a certain over prediction for higher frequencies. Therefore, the spectral shape of the simulated spectra differs from the measurements. One reason for the deviation of the computed from the measured spectral shape is assumed to be the two dimensional plane treatment of the acoustic propagation. Therefore, the acoustic refraction effects are approximately treated two dimensional, too. In jet flows acoustic waves are refracted at the strong density and velocity gradients of the mean flow. Refraction effects are dependent on frequency [36] and cause in cold, hot, and reacting jets the so called cone of silence, an area with reduced acoustic irradiation. The influence of refraction effects of the DLR-A mean flow gradients on the acoustics was numerically investigated by Bui et al. [36].

Computed acoustic intensity level spectra are compared to measurements [26] at the microphone positions #3 to #7 of the H3 flame in Fig. 8. The acoustic intensity level spectra were evaluated using a FFT of the computed pressure and velocity signals. Therefore, the computed sound pressure and velocity fluctuations with a real time of 0.2 s were split into intervals and their spectral distribution was computed using an

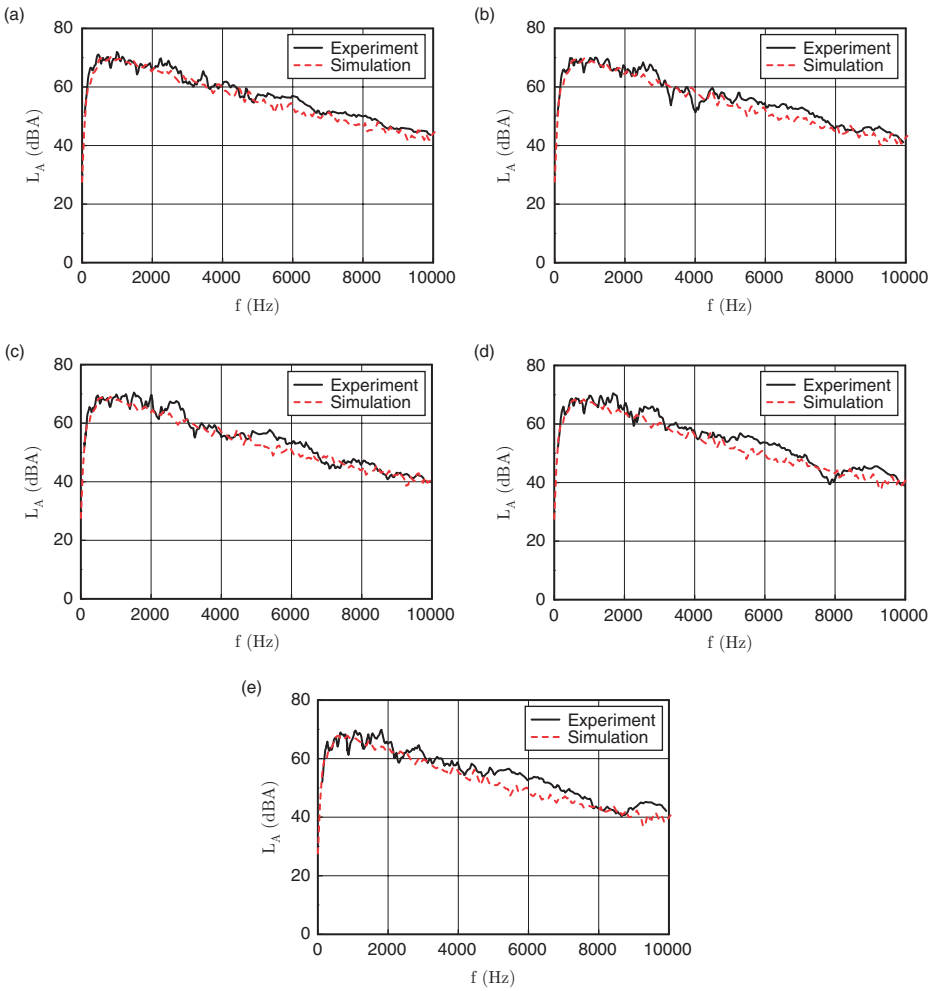

Figure 6: Measured and computed A-weighted sound pressure level spectra at the microphone positions #1 to #5 of the DLR-B flame. (a) #1 (25 D/0 D); (b) #2 (31 D/0 D); (c) #3 (37 D/0 D); (d) #4 (43 D/0 D); (e) #5 (50 D/0 D).

averaging procedure. A minimum frequency resolution of 100 Hz is achieved due to the Nyquist-Shannon sampling theorem. The intensity level spectra were computed with a narrow band spectrum of 1 Hz in accordance to the experimental data [26]. Analogously to the simulations of the DLR flames the combustion noise simulations of the H3 flame were conducted using the parameters $c_{Tl} = 0.273$, $c_{T\tau} = 1.864$, and $c_q = 251.19$ [10].

The combustion noise source modeling is discussed by the evaluation of the acoustic spectra at the microphone position #3. There, the combustion acoustics are least

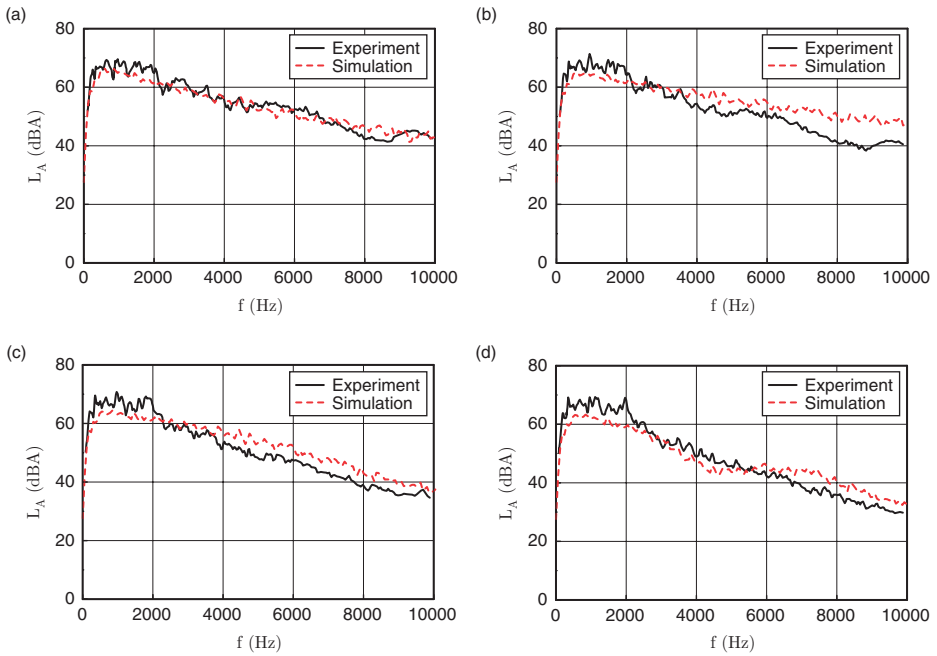

Figure 7: Measured and computed A-weighted sound pressure level spectra at the microphone positions #6 to #9 of the DLR-B flame. (a) #6 (50 D/12 D); (b) #7 (50 D/25 D); (c) #8 (50 D/37 D); (d) #9 (50 D/50 D).

affected by refraction effects because the detected acoustics pass the strong mean flow gradients of the flow field approximatively orthogonal. At this microphone location the computed intensity level spectrum agrees well with the experimental data for $f < 2500$ Hz. At higher frequencies the simulated acoustic intensity level is slightly over predicted and the spectral decay differs slightly from the measurements. Here, the computed acoustic intensity level spectra are not shifted into each other, too. This means, the RPM-CN approach in combination with the parameter set which was calibrated using the DLR-A and DLR-B flames computes acoustic intensity levels of the H3 flame that are in good accordance with experimental data.

The agreement of the computed with the measured acoustic intensity level spectra at the microphone location #4 and #5 is comparable with #3. The computed spectral shape at the microphone position #6 and #7 is in quite good accordance with the measured ones. However, the amplitudes are under predicted. One reason for the deviation of the computed from the measured acoustic intensity level spectra is expected to be the two dimensional plane treatment of the refraction effects.

In Fig. 9 the computed sound pressure level spectrum of the H3 flame is compared to the computed sound pressure level spectra of the DLR-A and DLR-B flames. The

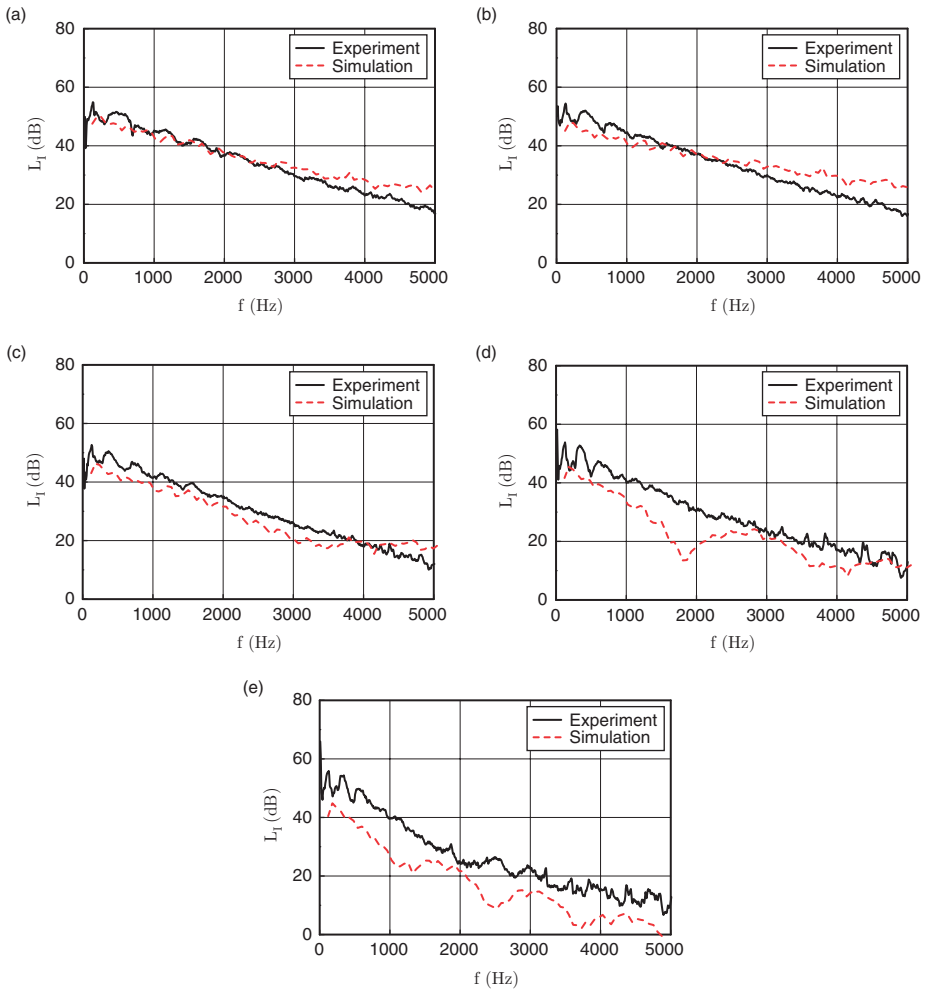

Figure 8: Measured and computed acoustic intensity level spectra at the microphone positions #3 to #7 of the H3 flame. (a) #3 (63 D/18 D); (b) #4 (63 D/43 D); (c) #5 (63 D/68 D); (d) #6 (50 D/80 D); (e) #7 (25 D/80 D).

computed sound pressure level spectrum of the H3 flame is computed analogously to the DLR flames and evaluated at the microphone position #1 of the DLR flames at $(x/r) = (25\ D/0\ D)$. The DLR-A and DLR-B flames have the identical geometrical setup and the same fuel composition (22, 1 Vol-% CH_4, 33, 2 Vol-% H_2, and 44, 7 Vol-% N_2). However, the flames differ in the mean jet exit velocity and therefore in their respective Reynolds number. The computed sound pressure level spectrum of the

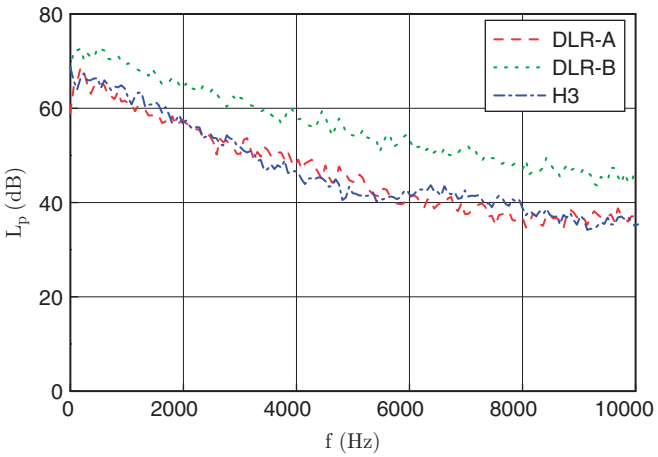

Figure 9: Computed sound pressure level spectra of the DLR-A, DLR-B, and H3 flames at the microphone position #1 (25 D/0 D).

DLR-B flame ($Re = 22800$) is increased about approximately 10 dB compared to the DLR-A flame ($Re = 15200$). Furthermore, the spectrum of the DLR-B flame has a slightly lesser decline toward higher frequencies. The setup of the H3 flame differs to the DLR flames in the fuel composition (50 Vol-% H_2 and 50 Vol-% N_2) and the mean jet exit velocity and therefore in its respective Reynolds number ($Re = 10000$). However, the computed sound pressure level spectra of the H3 flame have approximatively the same amplitudes and a similar spectral shape as the computed sound pressure level spectra of the DLR-A flame, in spite of the lower Reynolds number. This can be explained by the higher reaction rate of the nitrogen-diluted hydrogen flame compared to the nitrogen-methane-hydrogen fuel mixture. The higher reaction rate causes stronger combustion noise sources because the sources are accordingly to Eq. (4) a function of $\tilde{D}T''/Dt$.

Tam et al. [37] evaluated extensive experimental measurements to demonstrate that combustion noise from Auxiliary Power Units (APU) has a unique shape. The spectral shape which was found is the same as the F-Noise similarity spectrum of high-speed jet noise due to large turbulence structures [38]. Furthermore, Tam et al. [37] observed that the identified unique spectral shape of combustion noise of APUs is virtually the same as the shape of open jet flame combustion noise spectra. In Fig. 10 the computed combustion noise spectra of the DLR-A, DLR-B, and H3 flames are compared to the suggested similarity spectrum at the microphone location #1. For all flames, the simulated spectra are in quite good accordance with the F-Noise similarity spectrum. This means, the RPM-CN approach predicts combustion noise spectra of open non-premixed turbulent jet flames that are in accordance with the F-Noise similarity spectrum suggested by Tam et al. [37].

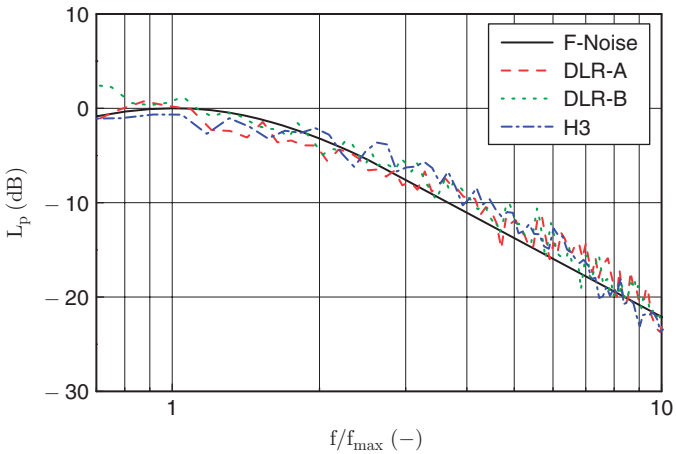

Figure 10: F-Noise similarity spectrum and computed sound pressure level spectra of the DLR-A, DLR-B, and H3 flames at the microphone position #1 (25 D/0 D).

6. CONCLUSIONS

The Random Particle-Mesh for Combustion Noise (RPM-CN) approach for the numerical simulation of broadband combustion noise was derived in a previous work and applied to three different open non-premixed turbulent jet flames in this work. The hybrid Computational Fluid Dynamics/Computational Aeroacoustics (CFD/CAA) approach relies on the stochastic reconstruction of combustion noise sources in the time domain. The Random Particle-Mesh (RPM) method is used for the modeling of the combustion noise sources out of statistical turbulence quantities, achieved by a steady Reynolds averaged Navier-Stokes (RANS) simulation. The modeled combustion noise sources are derived for the use in conjunction with the Linearized Euler Equations (LEE) for the computation of the acoustic propagation. The investigated DLR-A, DLR-B, and H3 flames are open non-premixed turbulent jet flame configurations which differ in the mean jet exit velocity, therefore in their respective Reynolds number, and in the fuel composition.

First, radial profiles of the axial velocity, the mixture fraction, the temperature, and the temperature Root Mean Square (RMS) were compared to measurements and discussed. The computed radial profiles of the reacting flow field are in acceptable agreement with the experimental data at very low computational costs. The certain deviations of the simulations and the measurements can be attributed to the steady simulation and the simplified modeling of turbulent structures.

Furthermore, sound pressure level spectra of the DLR-A and DLR-B flames and acoustic intensity level spectra of the H3 flame at different microphone locations were presented, compared to experimental data, and discussed. The very good agreement of

the computed sound pressure level spectra of the DLR-A and DLR-B flames at the microphone positions upstream in the fuel exit plane indicate the Reynolds scalability of the RPM-CN approach in combination with the parameter set for two dimensional plane conditions. This is certified by the additional good agreement of the computed and measured sound intensity level spectra of the H3 flame. At the microphone locations further downstream the fuel exit plane the computed combustion noise spectra of the DLR-A, DLR-B, and H3 flames show certain deviations regarding the shape compared to the experimental data. Since the source modeling is validated using the spectra at the microphone locations next to the source domain these certain deviations can be attributed to the modeling of acoustic propagation effects. One reason for these deviations is assumed to be the two dimensional plane modeling of the acoustics propagation effects, especially the acoustic refraction at the strong mean flow gradients of the reacting flow field.

This means, the quality of the reacting flow simulation by means of a steady RANS is sufficient as a basis for the combustion noise source modeling with RPM and the subsequently acoustic simulation using LEE due to the good agreement of computed and measured combustion noise spectra in these cases. The combustion noise source modeling was validated for open non-premixed turbulent jet flames by a very good agreement of computed combustion noise spectra with measurements next to the acoustic source zone. A more accurate modeling of the acoustic propagation, especially regarding the prediction of acoustic refraction effects, is assumed by a three dimensional treatment.

ACKNOWLEDGMENTS

This collaborative work was supported within the project AVANTGARDE which is funded by the German Aerospace Center (DLR).

REFERENCES

[1] T. Bui, W. Schröder, M. Meinke, Numerical analysis of the acoustic field of reacting flows via acoustic perturbation equations, Computers & Fluids 37 (9) (2008) 1157–1169.

[2] M. Ihme, D. Bodony, H. Pitsch, Prediction of combustion-generated noise in non-premixed turbulent jet flames using large-eddy simulation, in: AIAA 2006-2614, Cambridge, Massachusetts, 2006.

[3] F. Flemming, A. Sadiki, J. Janicka, Investigation of combustion noise using a LES/CAA hybrid approach, Proceedings of the Combustion Institute 31 (2007) 3189–3196.

[4] N. Andersson, L.-E. Ericsson, L. Dvidson, Large-eddy simulation of subsonic turbulent jets and their radiated sound, AIAA Journal 43 (9) (2005) 1899–1912.

[5] H. Brick, R. Piscoya, M. Ochmann, P. Költzsch, Hybride LES/Kirchhoff-Methode zur Berechnung des Verbrennungsgeräusches von freien Flammen (Hybrid LES/Kirchhoff-Method for the computation of combustion noise of open flames), in: DAGA 2005, Munich, Germany, 2005.

[6] A. Lyrintzis, Integral acoustics methods: From the (CFD) near-field to the (acoustic) far-field, International Journal of Aeroacoustics 2 (2) (2003) 95–128.

[7] W. Bechara, C. Bailly, P. Lafon, S. Candel, Stochastic approach to noise modelling for free turbulent flows, AIAA Journal 32 (3) (1994) 455–463.

[8] S. Klein, J. Kok, Sound generation by turbulent non-premixed flames, Combustion Science and Technology 149 (1) (1999) 267–295.

[9] C. Hirsch, J. Wäsle, A. Winkler, T. Sattelmayer, A spectral model for the sound pressure from turbulent premixed combustion, Proceedings of the Combustion Institute 31 (2007) 1435–1441.

[10] B. Mühlbauer, R. Ewert, O. Kornow, B. Noll, Evaluation of the RPM approach for the simulation of broadband combustion noise, AIAA Journal 48 (7) (2010) 1379–1390.

[11] R. Ewert, R. Emunds, CAA slat noise studies applying stochastic sound sources based on solenoidal digital filters, in: AIAA 2005-2862, Monterey, California, 2005.

[12] R. Ewert, RPM – the fast Random Particle-Mesh method to realize unsteady turbulent sound sources and velocity fields for CAA applications, in: AIAA 2007-3506, Rome, Italy, 2007.

[13] R. Ewert, Broadband slat noise prediction based on CAA and stochasic sound sources from a fast random particle-mesh (RPM) method, Computers & Fluids 37 (2008) 369–387.

[14] S. Pope, Turbulent flows, Cambridge University Press, Cambridge, United Kingdom, 2000.

[15] J. Garca-Ojalvo, J. Sancho, Noise in spatially extended systems, Springer-Verlag, New York, 1999.

[16] M. Billson, L.-E. Eriksson, L. Davidson, Jet noise prediction using stochastic turbulence modeling, in: AIAA 2003-3282, Hilton Head, South Carolina, 2003.

[17] C. Tam, L. Auriault, Jet mixing noise from fine-scale turbulence, AIAA Journal 37 (2) (1999) 145–153.

[18] P. Gerlinger, Numerische Verbrennungssimulation – Effiziente numerische Simulation turbulenter Verbrennung (Numerical combustion simulation – Efficient numerial simulation of turbulent combustion), Springer-Verlag, Berlin, Germany, 2005.

[19] R. Barlow (Ed.), Proceedings of the TNF Workshops, Sandia National Laboratories, Livermore, California, 1996–2004.

[20] V. Bergmann, W. Meier, D. Wolff, W. Stricker, Application of spontaneous Raman and Rayleigh Scattering and 2D LIF for the characterization of a turbulent $CH_4/H_2/N_2$ jet di3usion flame, Applied Physics 66 (4) (1998) 489–502.

[21] W. Meier, R. Barlow, Y.-L. Chen, Raman/Rayleigh/LIF measurements in a turbulent $CH_4/H_2/N_2$ jet diffusion flame: experimental techniques and turbulence-chemistry interaction, Combustion and Flame 126 (2000) 326–343.

[22] C. Schneider, A. Dreizler, J. Janicka, Flow field measurements of stable and locally extinguishing hydrocarbon-fuelled jet flames, Combustion and Flame 135 (2003) 185–190.

[23] K. Singh, S. Frankel, J. Gore, Study of spectral noise emissions from standard turbulent nonpremixed flames, AIAA Journal 42 (5) (2004) 931–936.

[24] D. Pfuderer, A. Neuber, G. Früchtel, E. Hassel, J. Janicka, Turbulence modulation in jet diffusion flames: Modeling and experiments, Combustion and Flame 106 (3) (1996) 301–307.

[25] M. Tacke, Zur Stabilität angehobener turbulenter Diffusionsflammen (On the stability of detached turbulent diffusion flames), Ph.D. thesis, Technische Universität Darmstadt (1998).

[26] R. Piscoya, H. Brick, M. Ochmann, P. Költzsch, Equivalent source method and boundary element method for calculating combustion noise, Acta Acous-tica united with Acoustica 94 (4) (2008) 514–527.

[27] A. Dreizler, Flame data base for turbulent nonpremixed flames, http://www.tudarmstadt.de (2008).

[28] ANSYS-Inc., ANSYS CFX-Solver, Theory – Release 11.0, Canonsburg, Pennsylvania (December 2006).

[29] N. Peters, Turbulent combustion – Cambridge monographs on mechanics, Cambridge University Press, 2000.

[30] M. Braun-Unko3, Private communications, german Aerospace Center (DLR), Institute of Combustion Technology, Chemical Kinetics Department (2007).

[31] B. Noll, Numerische Strömungsmechanik (Numerical fluid mechanics), Springer-Verlag, Berlin, Germany, 1993.

[32] J. Delfs, M. Bauer, R. Ewert, H. Grogger, M. Lummer, T. Lauke, Numerical simulation of aerodynamic noise with DLR's aeroacoustic code PIANO – PIANO manual version 5.2, Tech. rep., German Aerospace Center (DLR), Institute of Aerodynamics and Flow Technology, Technical Acoustics Department, Braunschweig, Germany (January 2007).

[33] C. Tam, J. Webb, Dispersion-relation-preserving finite difference schemes for computational acoustics, Journal of Computational Physics 107 (1993) 262–281.

[34] F. Hu, M. Hussaini, J. Manthey, Low-dissipation and low-dispersion Runge-Kutta schemes for computational acoustics, Journal of Computational Physics 124 (1996) 177–191.

[35] R. W. Bilger, The structure of turbulent non-premixed flames, Symposium (International) on Combustion 22 (1) (1988) 475–488.

[36] T. Bui, W. Schröder, Acoustic wave refraction in open turbulent flames, Acta Acoustica united with Acoustica 95 (2009) 440–447.

[37] C. Tam, N. Pastouchenko, J. Mendoza, D. Brown, Combustion noise of auxiliary power units, in: AIAA 2005-2829, Monterey, California, 2005.

[38] C. Tam, M. Golebiowski, J. Seiner, On the two components of turbulent mixing noise from supersonic jets, in: AIAA 96-1716, State College, Pennsylvania, 1996.